Effects of Remote Ligand Substituents on the Structures, Spectroscopic, and Magnetic Properties of Two-Coordinate Transition Metal Thiolate Complexes

Jade Pratt,[†] Aimee M. Bryan,[†] Michelle Faust,[†] Jessica N. Boynton,[†] Petra Vasko,[‡] Brian D. Rekken,[†] Akseli Mansikkamäki,[‡] James C. Fettinger,[†] Heikki M. Tuononen,[‡,*] and Philip P. Power[†,*]

[†] Department of Chemistry, University of California, Davis, One Shields Avenue, Davis, California 95616, United States

[‡] Department of Chemistry, Nanoscience Center, University of Jyväskylä, P.O. Box 35, FI-40014 University of Jyväskylä, Finland

ABSTRACT

The first row transition metal(II) dithiolates $M(SAr^{iPr4})_2$ (Ar^{iPr4} = C_6H_3-2,6-(C_6H_3-2,6-iPr_2)$_2$, M = Cr (**1**), Mn (**3**), Fe (**4**), Co (**5**), Ni (**6**), and Zn (**7**)), $Cr(SAr^{Me6})_2$ (**2**) (Ar^{Me6} = C_6H_3-2,6-(C_6H_2-2,4,6-Me_3)$_2$) and the ligand transfer reagent $(NaSAr^{iPr4})_2$ (**8**) are described. In contrast to their $M(SAr^{iPr6})_2$ (M = Cr, Mn, Fe, Co, Ni, and Zn; Ar^{iPr6} = C_6H_3-2,6-(C_6H_2-2,4,6-iPr_3)$_2$) congeners, which differ from **1** and **3** – **6** in having *para*-isopropyl groups on the flanking aryl rings of the terphenyl substituents, compounds **1** and **4** – **6** display highly bent coordination geometries with S–M–S angles of 109.802(2) (**1**), 120.2828(3) (**4**), 91.730(3) (**5**), and 92.68(2)° (**6**) as well as relatively close metal–flanking aryl ring η^6 interactions with metal–centroid distances of 2.11477(6) (**1**), 1.97188(3) (**2**), 2.15269(6) (**4**), 1.62058(9) (**5**), and 1.724(8) Å (**6**). However, the

d^5 (Mn) and d^{10} (Zn) complexes **3** and **7** display linear or near-linear coordination with no close metal–ligand distances. The non-linear geometries of **1** and **4** – **6** also contrast with those of their Ar^{iPr4} substituted alkoxo and amido congeners, which have strictly linear coordination. Complexes **1** – **7** were synthesized by the reaction of lithium or sodium thiolate salt with the metal dihalide or, in the case of **3**, by the reaction of the thiol with the amido complex $Mn[N(SiMe_3)_2]_2$. All compounds were characterized by electronic spectroscopy, X-ray crystallography, and magnetic measurements using Evans' method and SQUID magnetometry. It was concluded that, despite the large bulk of the Ar^{iPr4} substituents, the absence of *para*-isopropyl groups on the flanking rings of the ligand permits close secondary metal–flanking ring distances. The compounds are characterized by more intense colors and display magnetic moments that are generally lower than the spin-only values, in agreement with the covalent character of the close metal–flanking ring η^6 interactions.

INTRODUCTION

The achievement of strictly linear coordination in two-coordinate, open shell transition metal complexes is often difficult. Two-coordination has been obtained by the use of very sterically bulky ligands to prevent aggregation and/or decomposition via disproportionation,[1-3] but there are a few two-coordinate, open shell (d^1 – d^9), transition-metal complexes that have exactly linear geometry in the solid state.[1] Linear complexes, especially those of Fe^{2+} and Co^{2+}, are of interest because they often have unquenched orbital angular momentum and effective magnetic moments that approach free-ion values.[4-15] To date, two-coordinate complexes have been stabilized by aryloxide,[9,10,16] amido,[4,7,8,17-23] alkyl,[6,24-28] aryl[29-33], thiolato,[34,35] and carbene[36-46] ligands. The

bulkiest amido derivatives M{N(H)Ar^{iPr6}}$_2$ (M = V, Cr, Mn, Fe, Co, and Ni ; Ar^{iPr6} = C_6H_3-2,6-(C_6H_2-2,4,6-iPr_3)$_2$)[38] have linear or near-linear geometries, as do those of the related slightly less highly substituted ligand –N(H)Ar^{iPr4} (Ar^{iPr4} = (C_6H_3-2,6-(C_6H_3-2,6-iPr_2)$_2$), which does not have isopropyl substituents at the para positions on the flanking aryl rings.[4,20] The isoelectronic aryloxides, featuring the Ar^{iPr4} substituents, i.e. M(OAr^{iPr4})$_2$ (M = Fe and Co), also have linear geometries.[9,10] In contrast, complexes of ligands with the significantly less bulky terphenyl substituent (Ar^{Me6} = C_6H_3-2,6(C_6H_2-2,4,6-Me_3)$_2$) and the related Ar^{Me4} = C_6H_3-2,6(C_6H_3-2,6-Me_2)$_2$,[47] generally have severely bent coordination with relatively short metal–flanking ring interactions so that the metal–ligand environments can approach pseudotetrahedral.[4,8,10,19,34]

On the basis of the previous work with Ar^{iPr4} and Ar^{iPr6} substituted amido[4,8,19] or aryloxo[9,10] ligands, it was expected that the analogous thiolato ligand –SAr^{iPr4} would also induce linear or near-linear metal coordination like those of their bulkier counterparts M(SAr^{iPr6})$_2$ (M = Cr, Mn, Co, and Ni).[35] Herein, we report that this is not the case and describe the synthesis and characterization of seven new transition metal(II) thiolates: Cr(SAr^{iPr4})$_2$ (**1**), Cr(SAr^{Me6})$_2$ (**2**), Mn(SAr^{iPr4})$_2$ (**3**), Fe(SAr^{iPr4})$_2$ (**4**), Co(SAr^{iPr4})$_2$ (**5**), Ni(SAr^{iPr4})$_2$ (**6**), and their zinc analogue Zn(SAr^{iPr4})$_2$ (**7**). All except **3** and **7** have highly bent geometries with short metal–flanking aryl ring interactions. The reasons for these unexpected structural differences between the closely related ligand sets have been explored by DFT methods using the Cr(SAr)$_2$ (**9**) (Ar = C_6H_3-2,6-(C_6H_5)$_2$) model system and optimizing its structure both in linear and bent geometries. The calculations show that bending of the metal coordination geometry requires little energy with the energy differences between bent and linear geometries for **1** and **2** being just 10 and 17 kJ mol^{-1},

respectively. Also, the empirical dispersion correction had only a minor effect reducing the energy difference between the bent and linear forms by 6 and 10 kJ mol^{-1}. These findings and the earlier results reveal that the essentially linear geometries of the $M\{N(H)Ar^{iPr4}\}_2$,[4,20] $M\{N(H)Ar^{iPr6}\}_2$,[8,19] and $M(SAr^{iPr6})_2$[35] series of first row transition metal species are largely the result of steric conflict between the isopropyl substituents of the terphenyl rings. In contrast, for the thiolate ligand $-SAr^{iPr4}$, the larger size of sulfur and the resultant lowered steric restrictions permit bending to occur, which is driven by secondary interactions between the metal and the electron rich flanking ring whose effects only become apparent in the less crowded complexes $M(SAr^{iPr4})_2$. These effects are masked in the bulkier thiolate derivatives $M(SAr^{iPr6})_2$ where the seemingly remote *para*-isopropyl substituents prevent bending by steric blocking.[35]

EXPERIMENTAL SECTION

All manipulations were carried out under anaerobic and anhydrous conditions by using Schlenk techniques under a dinitrogen atmosphere or in a Vacuum Atmospheres HE-43 drybox. Solvents were dried by the method of Grubbs and coworkers,[48] stored over potassium or sodium, and then degassed by the freeze-pump-thaw method. All physical measurements were made under strictly anaerobic and anhydrous conditions. IR spectra were recorded as Nujol mulls between CsI plates on a Perkin-Elmer 1430 spectrometer. UV-visible spectra were recorded as dilute hexane or toluene solutions in 3.5 mL quartz cuvettes using an Olis 17 Modernized Cary 14 UV/Vis/NIR spectrophotometer or a HP 8452 diode array spectrophotometer. Melting points were determined on a MEL-TEMP II apparatus using glass capillaries sealed with vacuum grease. Unless otherwise stated, all materials were obtained from commercial sources and used as received.

$MnCl_2$ and $FeCl_2$ were dehydrated from $FeCl_2{\cdot}4H_2O$ and $MnCl_2{\cdot}6H_2O$ respectively, by following a similar dehydration procedure to that previously reported for $MnCl_2$.[49] The compounds $HSAr^{iPr4}$,[50] $LiSAr^{iPr4}$,[50,51] $LiSAr^{Me6}$,[51] $CrCl_2(THF)_2$,[52] and $Mn[N(SiMe_3)_2]_2$[49,53] were prepared by literature procedures.

$Cr(SAr^{iPr4})_2$ (1). Diethyl ether (*ca.* 30 mL) was added to a mixture of $CrCl_2(THF)_2$ (0.13 g, 0.49 mmol) and $LiSAr^{iPr4}$ (0.44 g, 1.0 mmol) at *ca.* −78 °C with rapid stirring. The resulting green solution was warmed to room temperature overnight and after stirring for *ca.* 2 d, the solvent was removed under reduced pressure. The residue was extracted with *ca.* 20 mL of toluene. The bright green solution was filtered concentrated to *ca.* 10 mL under reduced pressure. Storage for 3 days at *ca.* −18 °C gave green crystals of **1** suitable for X-ray diffraction study. Yield: 0.12 g (26 %). Mp 165 °C (dec). UV-Vis (hexanes, nm [ε, $M^{-1}cm^{-1}$]): 306 [3500], 362 [1000], and 437 [20]. IR in Nujol mull (cm^{-1}) with CsI plates: ν_{Cr-S} 390 (w). μ_{eff} in C_6D_6 solution = 4.96 μ_B.

$Cr(SAr^{Me6})_2$ (2). Diethyl ether (*ca.* 30 mL) was added to a rapidly stirred mixture of $CrCl_2(THF)_2$ (0.22 g, 0.82 mmol) and $LiSAr^{Me6}$ (0.58 g, 1.6 mmol) at *ca.* −78 °C. The resulting green solution warmed overnight to room temperature. After stirring for *ca.* 2 d, the solvent was removed under reduced pressure and the residue was extracted with *ca.* 30 mL of hexane. The bright green solution was filtered and concentrated to *ca.* 20 mL under reduced pressure. Storage for one week at *ca.* −32 °C gave green crystals of **2** suitable for X-ray diffraction. Yield: 0.20 g (32 %). Mp 110 °C (dec). UV-vis (hexanes, nm [ε, $M^{-1}cm^{-1}$]): 368 [1800], 416 [900], and 612 [100]. IR in Nujol mull (cm^{-1}) with CsI plates: ν_{Cr-S} 390 (w). μ_{eff} in C_6D_6 solution = 3.83 μ_B.

Mn(SAr^{iPr4})$_2$ (3). A solution of Ar^{iPr4}SH (0.91g, 2.0 mmol) in *ca.* 30 mL of hexanes was added dropwise to a solution of [Mn{N(SiMe$_3$)$_2$}$_2$]$_2$ (0.187g, 0.5 mmol) in *ca.* 20 mL of hexanes at room temperature and stirred for 6 days. Hexanes and HN(SiMe$_3$)$_2$ were removed under reduced pressure and the brown solid residue was triturated with *ca.* 15 mL of hexanes and re-dissolved (*ca.* 10 mL) hexanes to give light brown solution. Storage overnight at *ca.* 6 °C gave pale yellow crystals of **3** suitable for X-ray diffraction study. Yield: 0.357 g (39 %). Mp 231 – 233 °C. IR in Nujol mull (cm^{-1}) with CsI plates: ν_{Mn-S} 460, 385 (w). μ_{eff} in C_6D_6 solution = 5.82 μ_B.

Fe(SAr^{iPr4})$_2$ (4). A solution of (NaSAr^{iPr4})$_2$, **8**, (3.6 g, 4.0 mmol) in *ca.* 30 mL of THF was added dropwise to a suspension of $FeCl_2$ (0.51 g, 4.0 mmol) in *ca.* 20 mL of THF at 0 °C. The yellow suspension was warmed to room temperature and stirred for 4 days. THF was removed under reduced pressure from the resultant red solution. The orange-red residue was extracted with *ca.* 100 mL of hot hexanes to give a red solution with an orange precipitate. This precipitate was allowed to settle and the supernatant liquid was decanted and concentrated under reduced pressure to incipient crystallization. Standing at room temperature overnight gave **4** as red crystals that were suitable for X-ray diffraction. Yield: 0.44 g (12 %). Mp 210 – 212 °C. UV-vis: (toluene, nm [ε, M^{-1}cm^{-1}]): 331 [4000], 404 [2600], 445 [3100]. IR in Nujol mull (cm^{-1}) with CsI plates: ν_{Fe-S} 390 (w). μ_{eff} in C_7D_8 solution = 4.02 μ_B.

Co(SAr^{iPr4})$_2$ (5). A solution of (NaSAr^{iPr4})$_2$, **8**, (3.6 g, 4.0 mmol) in THF (*ca.* 35 mL) was added dropwise to a suspension of $CoCl_2$ (0.52 g, 4.0 mmol) in *ca.* 15 mL of THF at 0 °C, which produced an immediate color change from pale blue to purple. The solution was warmed to room

temperature and stirred for 4 days. THF was removed under reduced pressure to afford a dark-blue solid residue. This was extracted with *ca.* 60 mL of hot hexanes to give a dark blue solution with a pale blue precipitate. Filtration afforded a clear violet solution, which was concentrated under reduced pressure to incipient crystallization. Standing overnight at room temperature gave blue black crystals of **5** suitable for X-ray crystallography. Yield: 0.83 g (23 %). Mp > 260 °C. UV-vis (toluene, nm [ε, $M^{-1}cm^{-1}$]): 413 [2800], 498 [3100], 606 [2100], 806 [200], 1260 [300]. IR in Nujol mull (cm^{-1}) with CsI plates: ν_{Co-S} 350 (w). μ_{eff} in C_6D_6 solution = 3.29 μ_B.

Ni(SAr^{iPr4})$_2$ (6). A solution of (NaSAr^{iPr4})$_2$, **8**, (0.90 g, 1.0 mmol) in *ca.* 30 mL of diethyl ether was added dropwise to a suspension of NiI_2 (0.64 g, 1.2 mmol) in *ca.* 20 mL of diethyl ether at room temperature and stirred for 5 days. The mixture was filtered to afford a dark purple solution. Removal of solvent under reduced pressure afforded a dark purple solid residue which was redissolved in *ca.* 40 mL Concentration under low pressure and torage at *ca.* 6 °C for 3 days produced dark purple crystals of **6** that were suitable for X-ray diffraction. Yield: 0.294 g (32 %). Mp > 260 °C. UV-vis (hexanes, nm [ε, $M^{-1}cm^{-1}$]): 360 [1333], 445 [1215], 550 [1090]. IR in Nujol mull (cm^{-1}) with CsI plates: ν_{Ni-S} 380 (w). μ_{eff} in C_6D_6 solution = 1.62 μ_B.

Zn(SAr^{iPr4})$_2$ (7). A diethyl ether solution (*ca.* 50 mL) of LiSAr^{iPr4} (0.872 g, 2.0 mmol) was added dropwise to a suspension of $ZnCl_2$ (0.136 g, 1.0 mmol) in *ca.* 50 mL of diethyl ether at room temperature. The mixture was stirred for 3 days to yield a yellow, cloudy solution which was filtered and taken to dryness under reduced pressure. Extraction with *ca.* 30 mL of hot toluene and concentration under reduced pressure to *ca.* 10 ml. Upon storage for 2 days at *ca.*6

°C, colorless crystals of **7** were obtained that were suitable for X-ray diffraction study. Yield: 0.082 g (9 %). Mp > 290 °C. IR in Nujol mull (cm^{-1}) with CsI plates: ν_{Zn-S} 2712 (w), 1455 (s), 1365 (s).

$(NaSAr^{iPr4})_2$ (8). A solution of $HSAr^{iPr4}$ (19 g, 44 mmol) in *ca.* 125 mL of hexane was added to a flask containing sodium metal (2.0 g, 87 mmol) at room temperature. The colorless solution was refluxed for *ca.* 24 h. and cooled to room temperature to give a white precipitate which was allowed to settle. After removal of the pale-yellow supernatant liquid, the precipitate was washed with hexane and the solids were re-dissolved in diethyl ether (*ca.* 25 mL). Filtration and concentration to *ca.* 5 mL and storage at 6 °C afforded colorless crystals of **8** that were suitable for X-ray crystallography. Yield 16.2 g (82 %). Mp 230 – 232 °C. IR in Nujol mull (cm^{-1}) with CsI plates: 2918 (s), 1453 (m), 1370 (m), 798 (w), 715 (w). ^{1}H NMR (400 MHz, C_7D_8, 295 K): δ = 1.13 (d, 12H, *o*-CH(CH_3)$_2$), 1.19 (d, 12H, *o*-CH(CH_3)$_2$), 2.86 (m, 4H, *o*-CH(CH_3)$_2$), 7.03 (s, 4H, *m*-C_6H_3), 7.05 (s, 2H, *p*-C_6H_3), 7.09 (s, 2H, *m*-C_6H_3), 7.14 (s, 1H, *p*-C_6H_3).

X-ray Crystallography. Crystals suitable for X-ray diffraction studies were removed from the Schlenk tube under a flow of nitrogen and immediately covered with a layer of hydrocarbon oil. A single crystal was mounted on a glass fiber attached to a copper mounting pin and placed in a low-temperature nitrogen stream.[54] Data for **1**, **2**, **5**, and **7** were collected at 90(2) K with (λ = 1.5418 Å) Cu Kα_1, and data for **4** and **8** were collected at 90(2) K with (0.71073 Å) Mo Kα_1 radiation using a Bruker DUO diffractometer in conjunction with a CCD detector. Data for **3** were collected at 101 K with (0.71073 Å) Mo Kα_1, and data for **6** were collected at 100 K with (λ = 1.54178 Å) Cu Kα_1 radiation, using a Bruker Kappa diffractometer in conjunction with a CCD

detector. The collected reflections were corrected for Lorentz and polarization effects and for absorption by use of Blessing's method as incorporated into the program SADABS,[55,56] The structures were solved by direct methods and refined with the SHELXTL (2012, v.6.1) or SHELXTL (2013) software packages.[57] Refinement was by full-matrix least-squares procedures with all carbon-bound hydrogen atoms included in calculated positions and treated as riding atoms. The thermal ellipsoid plots were drawn using OLEX2 software.[58] A summary of crystallographic and data collection parameters is given in the SI.

Computational Details. All geometry optimization were carried out at DFT level using the PBE0 hybrid exchange correlation functional[59-62] and def2-TZVPP basis sets[63]. Grimme's DFT-D3 empirical dispersion correction[64,65] was used to model dispersion effects in geometry optimizations. Chromium was chosen as a model metal due to the availability of experimental solid-state structures for the three different ligands, $-SAr^{iPr6}$, $-SAr^{iPr4}$, and $-SAr^{Me6}$. Furthermore, the $Fe(SAr^{iPr4})_2$ and $Co(SAr^{iPr4})_2$ compounds have very similar bent geometries in the solid state to **1**. We assumed, therefore, that the calculated energies and trends for chromium compounds would be similar to their iron and cobalt analogues, and that similar reasons for the bending in the S–M–S (M = Cr, Fe, or Co) unit would apply. Because of the size of $-SAr^{iPr4}$ and $-SAr^{Me6}$ ligands in **1** and **2**, frequency calculations were not performed for the optimized geometries as this would have been prohibitively expensive in terms of CPU time. For this reason, and in order to investigate the energetics involved in the bending of the S–Cr–S unit, the model compound $Cr(SAr)_2$ (**9**, Ar = C_6H_3-2,6-(C_6H_5)$_2$) was calculated. Several model structures of the type $M(SPh)_2$ (M = Cr, Mn, Fe, Co, and Ni) were also optimized with various structural constraints to

study the magnetic properties of the complexes and their dependence on the structural parameters. The geometry optimizations of **1**, **2**, and **9** were conducted using the TURBOMOLE, version 6.3.1, program,[66] whereas the calculations for the $M(SPh)_2$ structures were carried out using the Gaussian 09, revision D.01, program.[67]

Effective magnetic moments were calculated using multireference ab initio methods. Static electron correlation was accounted using the complete active space self-consistent field (CASSCF) method.[68,69] The calculations were carried out on the model species $M(SPh)_2$ and $M(SC_6H_3\text{-}2,6\text{-}(C_6M_5))_2$ in different geometries (see SI for further details). An active space consisting of the five 3d orbitals and the required 3d electrons were used. All states in each possible multiplicity were solved in a single state-averaged calculation. Spin-orbit coupling (SOC) was introduced using quasi-degenerate perturbation theory (QDPT) approach,[70] where the matrix of the SOC operator is constructed in a basis of the CASSCF eigenstates, and the full Hamiltonian is then diagonalized to yield the spin-orbit coupled states and eigenvalues. Dynamic electron correlation outside the active orbital space was included using the quasi-degenerate *N*-electron valence state perturbation theory at the second order (NEVPT2) in its strongly contracted formulation.[71-74] Scalar relativistic effects were treated using the standard second-order Douglas-Kroll-Hess (DKH) transformation of the one-particle operator[75,76] along with the correct picture-change effects. The relativistically contracted DKH-def2-TZVPP basis was used for the metal ions and the DKH-def2-TZVP basis was used for other atoms.[77] All multireference calculations were carried out using the Orca, version 4.0.1, software.[78] The effective magnetic moments were calculated from magnetic susceptibility using standard expressions. The magnetic

susceptibility was calculated from the magnetic field derivatives of the electronic partition function as implemented in Orca.

RESULTS AND DISCUSSION

Synthesis and Spectroscopy. Compounds **1**, **2**, and **4** – **7** were synthesized in 9–39% yield by salt metathesis or ligand exchange. For **1** and **2**, the initial pale green color of the reaction mixtures slowly deepened to a forest green upon warming to room temperature. Stirring was continued for *ca*. 2 – 3 days to obtain better yields of the products. Crystals were grown at *ca.* −18 °C or −32 °C from toluene and hexane extracts of the dry reaction mixtures after filtration.

Compound **3** was obtained by the addition of 2 equiv of the thiol $Ar^{iPr_4}SH$[50] in hexanes to a hexane solution of $[Mn\{N(SiMe_3)\}_2]_2$[49,53] at room temperature, which produced a color change from pale pink to pale brown after stirring for 6 days. The crude product, obtained by evaporation of the solvent, was triturated with chilled hexanes, then re-dissolved in warm hexanes (*ca*. 20mL), concentrated, and stored overnight at *ca.* 6 °C for recrystallization.

Compounds **4** and **5** were obtained by slow addition of 1 equivof $(NaSAr^{iPr_4})_2$ in THF to a suspension of $FeCl_2$ or $CoCl_2$ in THF at 0 °C, which produced immediate color changes from pale yellow to red (**4**) and pale blue to violet (**5**). The sodium salt was chosen as the transfer agent because the low solubility of the eliminated sodium halide (in contrast to a lithium halide) tends to drive the reaction to completion. The reactions were initially attempted in diethyl ether, but no reactions were apparent. However, the addition of THF produced color changes almost

immediately, and stirring the reaction mixtures for *ca.* 3 – 4 days produced higher yields and purer products. Compound **4** crystallized immediately upon concentrating a hexane solution and standing overnight at room temperature. Obtaining pure compound **5** required careful recrystallization to separate the product from impurities. The ^{1}H NMR spectrum of compound **5** in benzene features a very small amount of terphenyl contaminant (see the SI for further details), consistent with the presence of $Ar^{iPr4}S–SAr^{iPr4}$ as a decomposition product via a redox process.

The nickel analog **6** was also synthesized in a similar manner to **3** and **4**. A solution of **8** in diethyl ether was added dropwise to a suspension of NiI_2 in diethyl ether at room temperature, and the solution was stirred for 5 days to yield a dark purple solution, which was filtered and extracted with hexanes. Crystals of **6** suitable for X-ray diffraction studies were obtained from a concentrated solution after 3 days storage at 6 °C.

Compound **7** was synthesized using similar conditions to those used for **1** and **2**. The colorless solution was stirred for 6 days. The ether was removed and the residue was extracted with toluene (10 mL). Suitable crystals for X-ray diffraction studies were obtained from a concentrated toluene solution after 2 days of storage at 6 °C.

The IR spectra of compounds **1** – **6** include M–S (M = Cr, Fe, Co, and Zn) vibrations between 350 and 390 cm^{-1}, which are consistent with published values for related complexes.[34,35] The UV-vis spectra are characterized by broad absorptions in the UV-visible region, which can be attributed to sulfur to metal electron charge transfer bands. Only compounds **5** and **6** display a well-defined *d-d* transition at longer wavelengths. These observations are similar to the reported

UV-vis spectra for previous thiolate species in that *d-d* transitions are only observed for Co^{2+} and Ni^{2+} but were not obsereved for Cr^{2+} or Fe^{2+} compounds.

Table 1. Comparison of UV-Vis Absoprtion Maxima (nm, [ε, $M^{-1}cm^{-1}$]) of $M(SAr^{iPr4})_2$ with those of $M(SAr^{iPr6})_2$.

Metal (M)	$M(SAr^{iPr4})_2$	$M(SAr^{iPr6})_2$
Cr (**2**)[a]	306 [3500], 362 [1000], 437 [20]	290 [200]
Fe (**4**)[b]	331 [4000], 404 [2600], 445 [3100]	385 [280]
Co (**5**)[b]	413 [2800], 498 [3100], 606 [2100], 806 [200], 1260 [300]	442 [130], 623 [185]
Ni (**6**)[a]	360 [1300], 445 [1200], 550 [1100]	450 [130], 503 [100], 864 [310]

[a] In hexanes. [b] In toluene.

Inspection of the data in Table 1 show the spectra of the $–SAr^{iPr4}$ derivatives have a greater number of bands that are also generally more intense than those of the corresponding $–SAr^{iPr6}$ derivatives. This is consistent with their lower symmetry and the greater number of metal–ligand interactions. The data also imply that the bent geometry is retained in solution. Thus the electronic spectra allow differentiation between the bent and linear structures in solution.

Structures. The solid state structures determined by single-crystal X-ray diffraction of compounds **1** – **7** are illustrated in Figures 1 – 7. Structural data are provided in Table 2 with average C–C distances within the interacting and non-interacting flanking rings being given in Table 3. The structure of **1** is illustrated in Figure 1. The data show that the chromium and sulfur atoms are disordered over two positions with 50 % metal occupancy at the sites Cr(1) and Cr(1a). The disordered sulfur afford different Cr-S distances, with the longer Cr–S distance

being associated with the terphenyl ligand exhibiting a close Cr–C interaction. The first coordination set may be regarded as containing S(1)–Cr(1)–S(1a) and the second set S(2)–Cr(1a)–S(2a). The Cr^{2+} ion also has a weak interaction with an aromatic ring. The Cr–S distances are 2.2912(11) (Cr(1)–S(1)) and 2.3124(9) Å (Cr(1)–S(2a)), and the distance between Cr and the centroid of the flanking ring is 2.11477(6) Å. The Cr–S bond distances in **1** are slightly shorter than the Cr–S bond length of 2.3505(5) Å in $Cr(SAr^{iPr6})_2$[35] or the average Cr–S bond length of 2.388 Å in $[Cr(SCH_2CH_2S)_2][NMe_4]_2$[79,80]. Previously published data on the only known two-coordinate chromium thiolate $Cr(SAr^{iPr6})_2$ revealed a crystallographically symmetrical structure that exhibits linear coordination at the metal.[35] In addition, the *ipso*-carbons of the central aryl rings of the terphenyl groups were found to form a coplanar array with the S–Cr–S unit. The structural results for **1** are dramatic in that the S–Cr–S angle becomes 109.802(2)° vs 180° in $Cr(SAr^{iPr6})_2$ and the chromium atom has relatively short metal–aryl ring interactions to one of the flanking rings.[35]

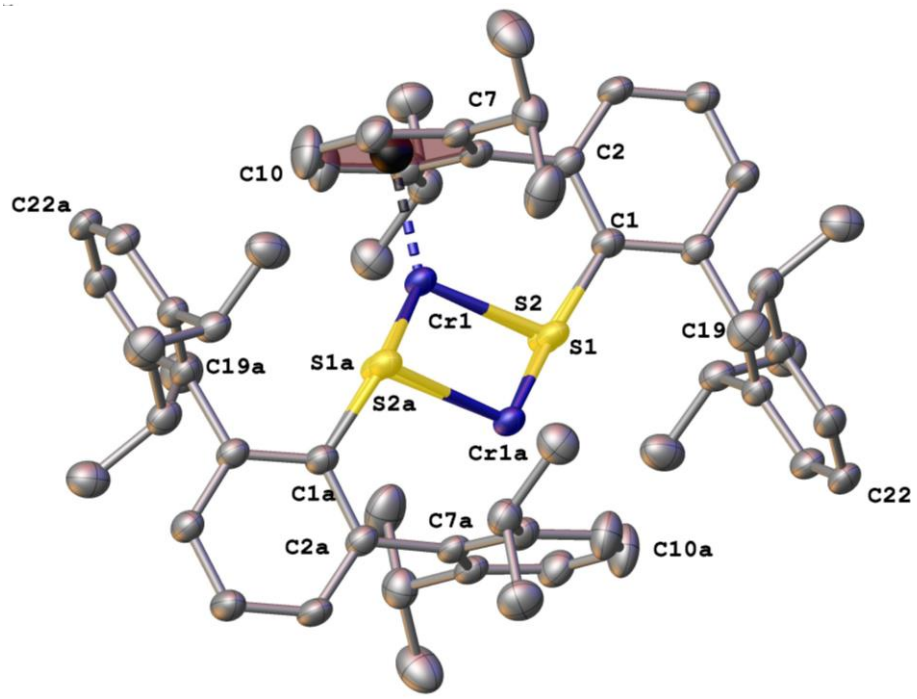

Figure 1. The X-ray crystal structure of $Cr(SAr^{iPr_4})_2$ (**1**). H atoms and solvent molecules are not shown, thermal ellipsoids are drawn at 50% probability. Both of the two disordered chromium positions are illustrated and the centroid of the C7 ring is indicated by a black sphere.

Table 2. Selected Interatomic Distances (Å) and Angles (°) for Compounds **1** – **8**.

Bond / Angle	$Cr(SAr^{iPr4})_2$ **(1)**[a]	$Cr(SAr^{Me6})_2$ **(2)**	$Mn(SAr^{iPr4})_2$ **(3)**	$Fe(SAr^{iPr4})_2$ **(4)**
M(1) – S(1)	2.2912(11)	2.31694(4)	2.3303(19)	2.29235(9)
M(1) – S(2,2a)	2.3124(9)	2.31909(3)		2.24725(9)
M(1) – centroid	2.11477(6)	1.97060(3)	2.8095(15)	2.15269(6)
S(1,1a) – M(1,1a) – S(2,2a)	109.802(2)	-	-	-
S(1) – M(1) – S(1,1a)	-	108.832(1)	180	120.2828(3)
M(1) – S(1) – C(1)	103.4(1)		104.80(8)	106.72(4)
M(1) – S(2) – C(31)	114.0(1)			120.28(4)
Σ^o M	359.99	358.09	-	351.48
Bond / Angle	$Co(SAr^{iPr4})_2$ **(5)**	$Ni(SAr^{iPr4})_2$ **(6)**	$Zn(SAr^{iPr4})_2$ **(7)**	$(NaSAr^{iPr4})_2$ **(8)**
M(1) – S(1)	2.1791(1)	2.1735(5)	2.1596(6)	2.7592(2)
M(1) – S(2,2a)	2.2678(1)	2.2056(5)	-	-
M(1) – centroid	1.62058(9)	1.724(8)	3.1850(2)	2.8127(2)
S(1) – M(1) – S(2,1a)	91.730(3)	92.68(2)	180	73.293(5)
M(1) – S(1) – C(1)	100.6(1)	100.64(6)	109.86(7)	-
M(1) – S(2) – C(31)	124.7(1)	124.19(6)		
Σ^o M	354.72	356.60	-	-

[a] Only one set of Cr–S distances from one of the two crystallographically independent molecules is given.

Table 3. Average C–C Bond Distances (Å) in Flanking Aryl Rings of $M(SAr^{iPr4})_2$.[a]

Metal (M)	Interacting Aryl Ring	Non-Interacting Aryl Ring of Same Terphenyl Substituent	Aryl Ring of Non-Interacting Terphenyl Substituent
Cr	1.406(8)	1.388(2)	1.391(9)
Mn	1.399(1)	1.397(8)	-
Fe	1.406(1)	1.397(7)	1.398(5)
Co	1.412(9)	1.396(4)	1.394(4)
Ni	1.410(7)	1.395(9)	1.394(2)
Zn	1.400(8)	1.398(3)	-

[a] The average C–C bond distances are lengthened in the interacting flanking aryl rings of complexes **1** – **7** in comparison to those in the non-interacting aryl ring.

Compound **2** crystallizes with two unique molecules per asymmetric unit. Due to their structural similarity, only the Cr (1) containing structure is discussed here; the structural parameters of the Cr (2) species are given in the SI. The structure of **2** (Figure 2), like **1**, features bent coordination at the metal. Due to the less bulky Ar^{Me6} substituents, a decrease in the S–Cr–S angle to 108.832(1)° is observed. The Cr–S bond distances in **2** are 2.31694(4) and 2.31909(3) Å which are marginally longer than those in **1**. The distance between the metal and the centroid of the flanking aryl rings, 1.97060(3) Å, is the shortest observed in Cr^{2+} terphenyl thiolates. The C–C bond lengths within the flanking terphenyl rings are consistent with the retention of aromaticity, unlike in e.g. $Ti\{N(H)Ar^{iPr6}\}_2$, where an alternating pattern of C–C distances is seen within the flanking aryl ring that interacts with the metal.[19] The chromium aryl ring interactions (average distance 2.337 Å) in the compound $Cr\{N(H)Ar^{Me6}\}_2$ are longer than those in **2**.[20]

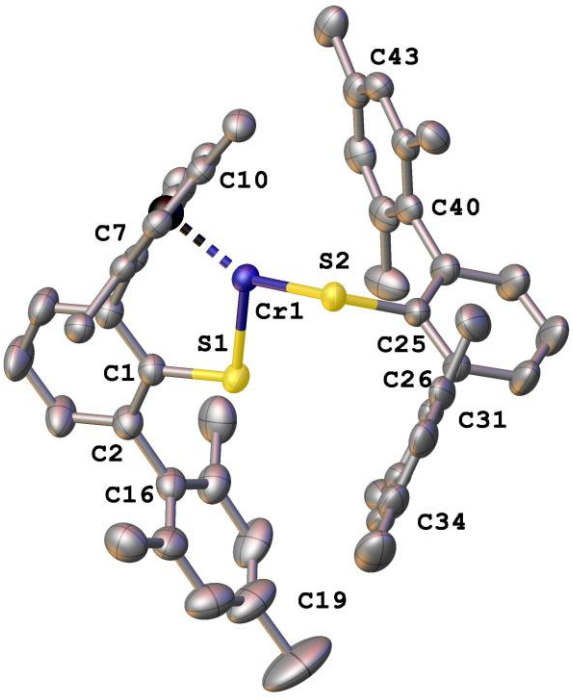

Figure 2. The X-ray crystal structure of $Cr(SAr^{Me6})_2$ (**2**). H atoms are not shown, thermal ellipsoids are at 50% probability, and the centroid of the C7 ring is indicated by a black sphere.

The manganese complex **3** (Figure 3) shows that the Mn atom is disordered over two positions (Mn1 and Mn1a) with atom each having 50 % occupancy. The S1–Mn–S1a angle is almost linear and the Mn–S distance is 2.3303(19) Å. Both the long Mn–centroid distance, 2.8095(15) Å, and the aromatic C–C bond lengths within the ring indicate very weak (if any) Mn–η^6 arene interactions. The only other known monomeric two-coordinate Mn(II) thiolate is $Mn(SAr^{iPr6})_2$, which also has linear coordination at the manganese atom and a Mn–S distance of 2.3041(7) Å.[35]

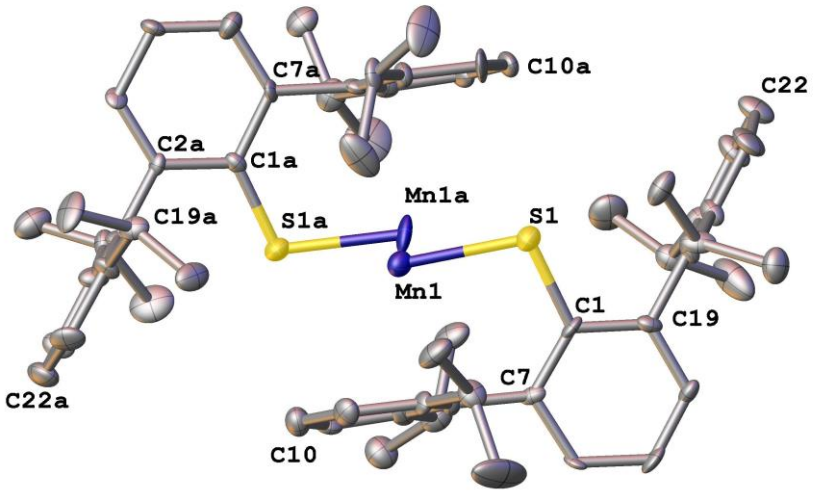

Figure 3. The X-ray crystal structure of $Mn(SAr^{iPr4})_2$ (**3**). H atoms are not shown for clarity, thermal ellipsoids are drawn at 50% probability. Both of the two disordered manganese positions are illustrated.

The iron complex **4** is illustrated in Figure 4. It features a short Fe–centroid distance of 2.15269(6) Å to the C7 flanking ring. Unlike the structure of $Fe(SAr^{iPr6})_2$, which has an inversion center, in the structure of **4**, the iron atom has flattened pyramidal coordination to two sulfur atoms and the centroid of the flanking ring (Σ° Fe = 351.48°). The two Fe–S distances in **4** are 2.29235(9) and 2.24725(9) Å, and are within the known range of Fe–S single bond lengths in two-coordinate iron-thiolates (2.1867(6) – 2.3517(6) Å).[34,35,47] The Fe–centroid distance, 2.15269(6) Å, is similar to those in $Fe(SAr^{iPr6})_2$ and $Fe(SAr^{Me6})(SC_6H_3\text{-}2,6(SiMe_3)_2)$.[35,47] In contrast, the less crowded complexes $Fe(SAr^{Me4})_2$ and $Fe(SAr^{Me4})_2$ generate pseudo-tetrahedral geometries at iron with short interactions to two flanking aryl rings featuring *ipso*-carbon-iron distances of 2.437 and 2.667 Å for $Fe(SAr^{Me4})_2$, and 2.636 and 2.535 Å for $Fe(SAr^{Me6})_2$.[34,47] The structure of **4** is in sharp contrast to their oxo- and amido-terphenyl analogs, $Fe(OAr^{iPr4})_2$ and $Fe\{N(H)Ar^{iPr4}\}_2$, which have linear L–Fe–L (L = OAr^{iPr4} or $N(H)Ar^{iPr4}$) coordination with much longer iron–flanking ring centroid distances of 3.0614 and 3.0861 Å.[5,9]

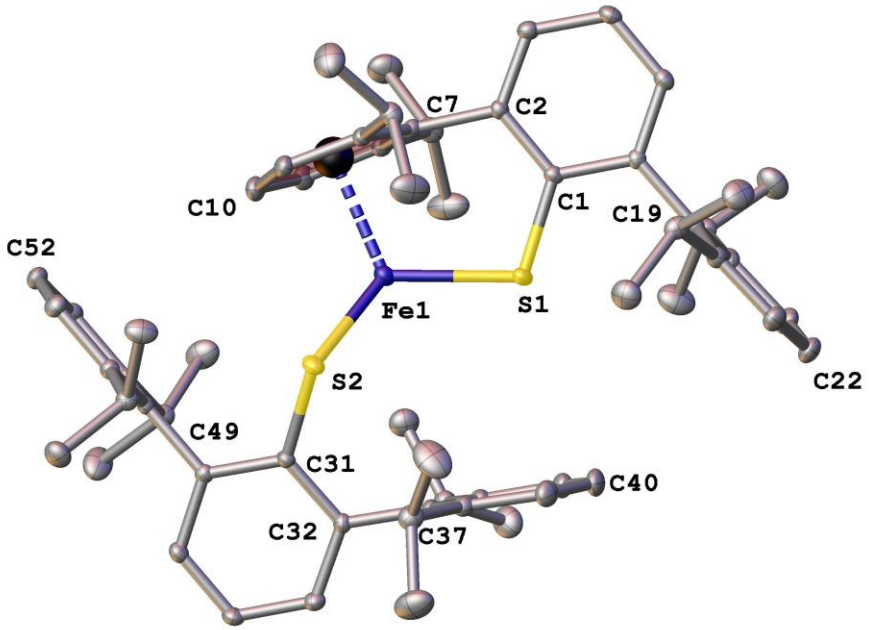

Figure 4. The X-ray crystal structure of Fe(SAr^{iPr4})$_2$ (**4**). H atoms are not show, thermal ellipsoids are at 50% probability, and the centroid of the C7 ring is indicated by a black sphere.

Compound **5** (Figure 5) displays a strongly bent cobalt coordination as indicated by its almost right-angle S1–Co1–S2 value of 91.730(3)°. The Co–S bond lengths are 2.1791(1) and 2.2677(1) Å. The shorter of the two distances is to S (1) which carries the terphenyl whose flanking ring displays a short Co–flanking aryl ring centroid distance of 1.62058(9) Å, and lengthened aromatic ring C–C bonds that salso indicate a strong Co–η^6 arene interaction.[81,82] The plane formed by the two sulfurs, cobalt, and the flanking ring centroid deviates slightly from trigonal planar geometry ($\Sigma°$ Co = 354.72°). The only other known monomeric two-coordinate cobalt(II) thiolate is Co(SAr^{iPr6})$_2$,[35] which has almost linear cobalt coordination (179.52(2)°), Co–S distances of 2.1912(6) and 2.1939(5) Å, and secondary Co–C7(*ipso*) distances of 2.665(3) and

2.660(3) Å. The metal–centroid interaction is also comparable to M–η^6 arene interactions (Fe– and Co–centroid distances 1.7625(19) and 1.7638(16) Å,) in the dimetal species $(MAr^{iPr4})_2$.[81,82]

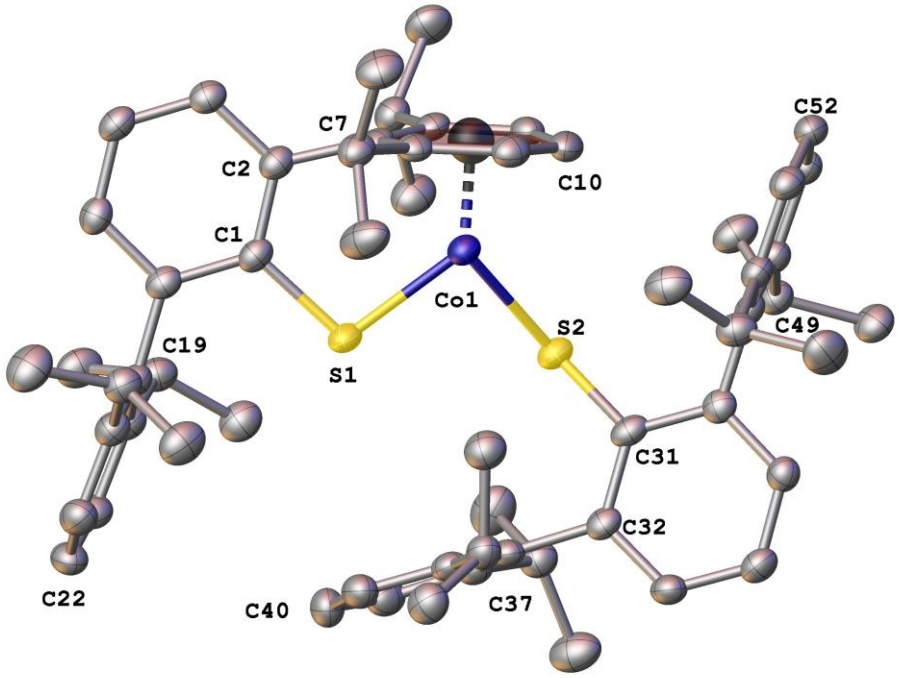

Figure 5. The X-ray crystal structure of $Co(SAr^{iPr4})_2$ (**5**). H atoms are not shown, thermal ellipsoids are at 50% probability, and the centroid of the C7 ring is indicated by a black sphere.

Complex **6** (Figure 6) has a strongly bent S1–Ni1–S2 angle of 92.68(2)°. The Ni–S distances 2.531(14) and 2.1735(5) Å differ greatly. However, the shorter of the two distances is to the terphenyl group with the flanking aryl ring—Ni interaction. The close Ni–centroid distance, 1.724(8) Å, and the aromatic C–C bond lengths in the ring also support this view. The two sulfur atoms, the nickel atom, and the centroid yield almost trigonal planar geometry (Σ° Ni = 356.60°).

The only other known monomeric two-coordinate nickel(II) thiolate Ni(SAr^{iPr6})$_2$ has almost linear coordination at the nickel atom (174.22(6)°) with Ni–S distances of 2.175(2) and 2.172(2) Å and secondary Ni–C-distances of 2.657(5) and 2.640(5) Å.[35]

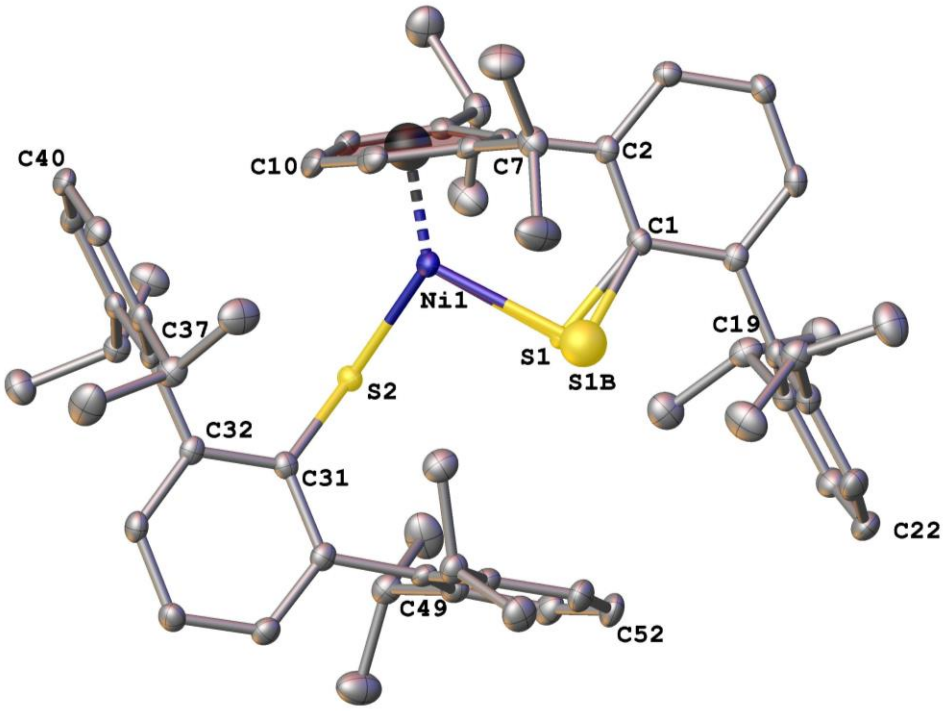

Figure 6. Thermal ellipsoid plot (50%) of Ni(SAr^{iPr4})$_2$ (**6**) with a disordered sulfur atom. H atoms are not shown, thermal ellipsoids are drawn at 50% probability, and the centroid of the C7 ring is indicated by a black sphere.

Compound **7** (Figure 7) is centrosymmetric with one half of the molecule being symmetry generated. The S1–Zn1–S1a angle is strictly linear at 180°. The Zn–S distance is 2.1596(6) Å. The long Zn–centroid distance, 3.1850(2) Å, and the C–C bond lengths of the aromatic ring indicate little or no Zn interactions with the flanking ring. The only other known monomeric two-

coordinate zinc(II) thiolate is $Zn(SAr^{iPr6})_2$, which has linear coordination at the zinc atom and a slightly longer Zn–S distance of 2.182(1) Å.[35]

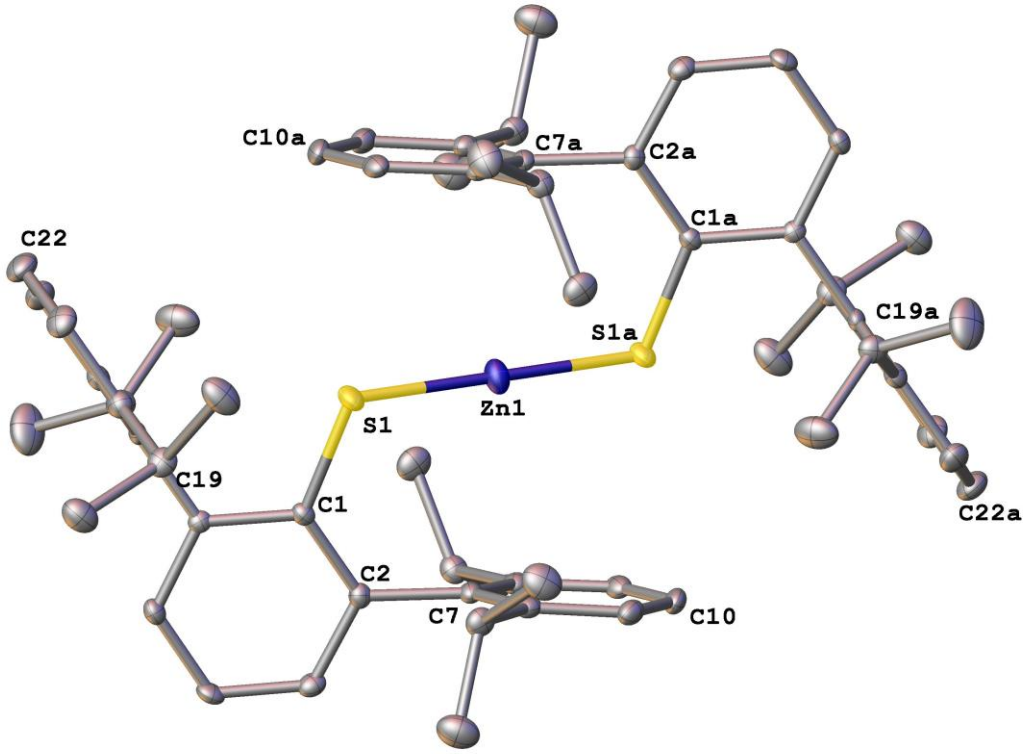

Figure 7. The X-ray crystal structure of $Zn(SAr^{iPr4})_2$ (**7**). H atoms are not shown and thermal ellipsoids are drawn at 50% probability.

The structure of compound **8** ($(NaSAr^{iPr4})_2$), is illustrated in the SI (Figure S24), has a dimeric structure and Na_2S_2 core similar to those of $(NaSAr^{iPr6})_2)$[50] and $(LiSAr^{iPr6})_2)$[50]. The Na-Centroid distance is 3.1059(15) Å.

In summary, the structures of compounds **1**, **2**, and **4** – **6** show that they display highly bent S–M–S geometries with moderately strong M–arene interactions as indicated by the short M–centroid distances and lengthened aryl C–C distances in the metal-interacting rings. These structural features are in contrast to those of the corresponding –SAr^{iPr6} derivatives, which have linear or near-linear coordination and weak metal–arene interactions. The differences show that the absence of a seemingly remote and unimportant *para*-isopropyl groups on the flanking aryl rings allows large changes in the coordination geometry at the metal. The linear coordination in the manganese and zinc complexes **5** and **7** is also consistent with minimal metal–flanking ring interactions even though such interactions would be sterically permitted. Further computational studies including combination of model compounds of different metals and related aryloxide and arylamido ligands are underway to further understand these factors and their implications.

Magnetic Measurements. The effective magnetic moments of complexes **1** – **6** were measured using Evans' method.[83] The magnetic moments of compounds **4** and **5** were also measured using a Quantum Design MPMSXL7 to provide corroboration for the values measured by Evans' method. The moments, 4.02 μ_B and 3.69 μ_B for **4** and **5**, respectively, at 300 K, are lower than the spin-only values of 4.90 μ_B for Fe and 3.87 μ_B for Co. The values are uncharacteristic for two-coordinate Fe and Co complexes that generally display magnetic moments significantly greater than the spin-only value, because of significant contributions from angular momentum. This suppression of magnetic moments is most likely due to the strong M–arene interactions, which effectively quenches orbital magnetism, unlike the almost free ion μ_B values in some linear species.[4-8]

The results and the respective spin-only values are listed in Table 4. It is clear that with the exception of **1** the observed values are less than the spin-only values. This is especially striking in the d^6 – d^8 complexes where orbital angular momentum effects are expected to generate moments that are much greater than the spin-only values.[4-8] The lower magnetic moments in **4**, **5**, and **6** may be contrasted with the higher values of 4.88, 5.75, and 2.58 μ_B in the corresponding linear or near-linear $M(SAr^{iPr6})_2$ (M= Fe, Co, and Ni) species.[35] The opposite is expected in the d^4 complexes **1** and **2** where the orbital and spin moments are in opposition. The lower than expected moments correspond to short distances between the metals and the flanking aryl ring. It is therefore reasonable to assume that the decrease in the moments, below the spin-only value, results from covalent interactions between the metal and the flanking aryl group, stabilizing a low-spin state. Nonetheless, DFT calculations demonstrate that the interactions between the metal ion and the flanking aryl ring lead only to a very small energy differences compared to a pseudolinear structure, where such interactions are absent. Linear structure (d^6, d^7, or d^8) would be expected to have moments higher than the spin-only value due to orbital contributions. Thus, even though the structures may be fluxional in solution, the lower than spin-only values suggest that even weak secondary metal ligand interactions can lower the magnetic moments effectively.

Table 4. Magnetic Moments of Complexes **1** – **6** as Measured with the Evans' Method (μ_B) and the Respective Spin-Only Values.

	1	**2**	**3**	**4**	**5**	**6**
Measured	4.96	3.83	5.82	3.95 4.02[a]	3.17 3.29[a]	1.62
Spin-only	4.90	4.90	5.92	4.90	3.87	2.83

[a] Magnetic moment measured using a Quantum Design MPMSXL7 superconducting quantum interference magnetometer.

Computations. To further investigate the reasons for the bending of the S–Cr–S unit in **1** and **2**, dispersion corrected PBE0/def2-TZVPP DFT calculations were performed first for the simplified model system **9** in which the flanking rings are phenyl groups. A stable minimum geometry was achieved by breaking the symmetry and optimizing the structure without symmetry constraints. This led to bending of the S–Cr–S angle from strictly linear geometry to 157.1°. However, despite such distortion, the energy difference between the bent minimum and linear transition state was found to be only 5 kJ mol^{-1}, thereby demonstrating that the energy required for bending of the S–Cr–S angle is very small. Similar results were obtained whether the calculations used the empirical dispersion correction or not. The dispersion correction was also found to have little effect on the optimized bond angles and bond lengths (see SI for further details), which is entirely expected as **9** contains the parent terphenyl ligand.

To quantify the effect of steric bulk of the terphenyl substituents on the calculated energies, the structures of **1** and **2** were optimized in both bent and linear geometries. The results show that the bent structure is always energetically preferred with the linear form residing 10 and 17 kJ mol^{-1} higher for **1** and **2**. The empirical dispersion correction has only a minor effect on the calculated energies, and reduced the energy difference between the bent and linear forms to 6 and 10 kJ mol^{-1} for **1** and **2** respectively. Although the computational data indicate that the bent structure is intrinsically favored over the linear, the energy differences are small and prevent any definitive statement to be made, especially because no frequency data are available. The calculations show that dispersion interactions do not play a decisive role in determining the structures of **1** and **2**.

A comparison of the dispersion corrected bent geometries of **1** and **2** to the crystallographically determined metrical parameters, reveals only slight discrepancies from the experimental data. Though the calculated Cr(1)–S(1) bond lengths (2.302 (**1**) and 2.307 Å (**2**)) are in good agreement with the experimental values, larger differences are observed in the S(1)–Cr(1)–S(2) angles that are slightly narrower in the optimized structures (104.7° for both (**1**) and (**2**)) than that observed crystallographically (109.802(2)^{o} (**1**) and 108.832(1)° (**2**)). Furthermore, the calculated Cr(1)–S(1)–C(1) angle in **1,** 103.2°, differs considerably from the experimental 121.126(2)°, which may be due to the structural disorder; the same bond angle is predicted within 1° of its experimental value for **2**. We also note that the theoretically predicted orientation of the ligands in both **1** and **2**, and especially that of their flanking rings, is comparable to the crystal structures. For example, the calculated interactions between the chromium and the *ipso*-carbon are 2.337 (**1**) and 2.353 Å (**2**), and are very close to the distances observed in the X-ray structure (Table 2).

The most probable reason for the observation of linear coordination for $Cr(SAr^{iPr6})_2$ is the steric hindrance caused by the bulky Ar^{iPr6} substituents that carry an isopropyl group at the *para* position in addition to those in the *ortho* positions of the flanking rings of the terphenyl group. Some of the steric differences between $-SAr^{iPr4}$ and $-SAr^{iPr6}$ are apparent from a representation of **1** with $-SAr^{iPr4}$ ligands (Figure 8), which shows that the *para* position is congested in the bent structure and is unlikely to easily accommodate a *para*-isopropyl group. To test this hypothesis, the structure of $Cr(SAr^{iPr6})_2$ was optimized in both bent and linear geometries with dispersion corrected DFT. In good agreement with the prediction, the linear structure was found to be lower in energy by 14 kJ mol^{-1}. Further computational studies for a combination of model compounds

with different metals and aryloxide and arylamido ligands are currently underway to understand the factors determining their geometries in the solid state.

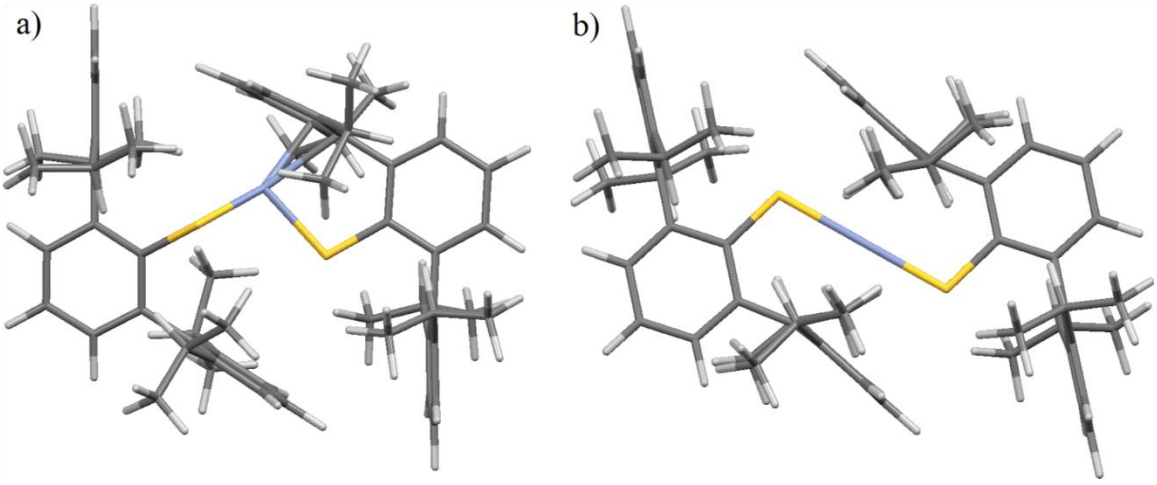

Figure 8. The structures of the Cr dithiolate $Cr(SAr^{iPr4})_2$ **1** in a) bent and b) linear geometry at the PBE0/def2-TZVPP level of theory. Color codes: blue (Cr), yellow(S), gray(C), white(H).

To clarify the contribution from different electron configurations to the observed effective magnetic moments, further calculations were carried out to compare the spin-state energetics. The calculations were performed for SAr^{iPr6} complexes **1** and **3** – **6**, which have been characterized for all of the studied metal ions. As discussed earlier, the observed effective magnetic moment most likely arises from numerous different conformations present in the solution. The number of such structures can be extremely large and it is thus not feasible to try and optimize all of them. Instead, the magnetic properties were studied by using the crystal structure geometries and simplified model structures. In the geometries extracted from the crystal

structures, the isopropyl groups were replaced by hydrogen to reduce the computational cost. Although these groups play an important role in the energetics of the different geometries, they do not carry any spin density, and therefore their contribution to the relative energies of different spin states and electron configurations evaluated at a fixed geometry is likely to be small.

In essence, the calculations for **1** and **3** afford μ_{eff} values for the D_{2h}, C_{2h}, bent, and full geometry models that are in good agreement with the measured μ_{eff} values and spin-only values (see SI for further details). For the iron species **4**, the calculated μ_{eff} of 5.2 μ_B for the full geometry produces the closest agreement with the measured value near 4.0 μ_B. However, the D_{2h}, C_{2h}, and bent geometries all produce significantly higher μ_{eff} values near 6.0 μ_B. For the cobalt species **5**, the full geometry calculated value of 2.5 μ_B is less than the experimental value 3.8 μ_B, whereas in the nickel species **6** the calculated value for the full geometry, near 3.0 μ_B, exceeds the experimental value of 1.6 μ_B. Although the results for the late d-block derivatives **4**, **5**, and **6** appear to support the view that bending the geometry lowers μ_{eff} and the secondary M–aryl interactions lower it further,[8] the effective magnetic moment is lower than the spin-only value only in the case of the cobalt species **5**, which also displays the strongest M–aryl interactions.

CONCLUSIONS

In summary, we have structurally and spectroscopically characterized six new transition metal(II) bis(thiolato) derivatives **1** – **6**, their zinc congener **7**, and the synthetically useful sodium arylthiolate transfer agent **8**. In sharp contrast to the derivatives of the related –SAr^{iPr6} ligand, the divalent metal –SAr^{iPr4}, except the d^5 (Mn^{2+}) and d^{10} (Zn^{2+}) derivatives **3** and **7**, feature strongly

bent coordination and close metal–flanking ring interactions of varying strength; the cobalt (II) species has the shortest such interaction with a Co–centroid distance of 1.62058(9) Å. Effective magnetic moments indicate mostly quenched orbital angular momentum in the compounds, which is consistent with their bent structures and a covalent interaction between the metal ion and flanking aryl ring. Although the DFT calculations indicate that the bent structure is intrinsically favored over a linear one because of metal–ligand interactions, it is the absence of the seemingly remote *para*-isopropyl substituents and the ligand flexibility permitted by the larger sulfur ligating atom (cf. –NHAr^{iPr4} [4,20] and –OAr^{iPr4} [9,10] ligands) that allows the bending to occur.

ASSOCIATED CONTENT

Supporting Information

Selected ^{1}H NMR, IR, and UV-vis spectra; selected interatomic distances and angles for the second molecule of **2** in its unit cell; X-ray crystallographic data collection parameters and selected bond distances and angles; xyz-coordinates of optimized geometries; and CIFs for compounds **1** – **8** (CCDC numbers 1555896 155898- 1555903 and 1828738). This material is available free of charge via the Internet at http://pubs.acs.org.

AUTHOR INFORMATION

Corresponding Author

E-mail: pppower@ucdavis.edu; ORCID: 0000-0002-6262-3209

E-mail: heikki.m.tuononen@jyu.fi; ORCID: 0000-0002-4820-979X

Notes

The authors declare no competing financial interest.

ACKNOWLEDGEMENTS

We thank the National Science Foundation (NSF) for financial support (Grants CHE-1263760 and CHE-1565501) and for the dual-source X-ray diffractometer (Grant 0840444). H.M.T. and A.M. thank the Academy of Finland (Grant 289172) and University of Jyväskylä for funding. P.V. thanks the Fulbright Center for a scholarship. A.M.B. thanks the NSF Graduate Research Fellowship Program for financial support (Grant DGE-1148897). We thank Mr. Jackson Badger, Professor Valentin Toufour and Dr. Peter Klavins for invaluable assistance in the collection of SQUID data for the cobalt complex.

REFERENCES

1. Power, P. P., Stable Two-Coordinate, Open-Shell (d^1–d^9) Transition Metal Complexes. *Chem. Rev.* **2012**, *112*, 3482-3507.
2. Kays, D. L., Recent Developments in Transition Metal Diaryl Chemistry. *Dalton Trans*. **2011,** *40*, 769-778.
3. Power, P. P., Some Highlights from the Development and Use of Bulky Monodentate Ligands. *J. Organomet. Chem.* **2004,** *689*, 3904-3919.

4. Bryan, A. M.; Merrill, W. A.; Reiff, W. M.; Fettinger, J. C.; Power, P. P., Synthesis, structural, and magnetic characterization of linear and bent geometry cobalt(II) and nickel(II) amido complexes: evidence of very large spin-orbit coupling effects in rigorously linear coordinated Co^{2+}. *Inorg. Chem.* **2012**, *51*, 3366-3373.
5. Zadrozny, J. M.; Atanasov, M.; Bryan, A. M.; Lin, C.-Y.; Rekken, B. D.; Power, P. P.; Neese, F.; Long, J. R., Slow Magnetization Dynamics in a Series of Two-Coordinate Iron (II) Complexes. *Chem. Sci*. **2013,** *4*, 125-138.
6. Reiff, W. M.; LaPointe, A. M.; Witten, E. H., Virtual Free Ion Magnetism and the Absence of Jahn−Teller Distortion in a Linear Two-Coordinate Complex of High-Spin Iron(II). *J. Am. Chem. Soc.* **2004**, 126, 10206-10207.
7. Reiff, W. M.; Schulz, C. E.; Whangbo, M.-H.; Seo, J. I.; Lee, Y. S.; Potratz, G. R.; Spicer, C. W.; Girolami, G. S., Consequences of a Linear Two-Coordinate Geometry for the Orbital Magnetism and Jahn−Teller Distortion Behavior of the High Spin Iron(II) Complex $Fe[N(t\text{-}Bu)_2]_2$. *J. Am. Chem. Soc.* **2009**, *131*, 404-405.
8. Merrill, W. A.; Stich, T. A.; Brynda, M.; Yeagle, G. J.; Fettinger, J. C.; De Hont, R.; Reiff, W. M.; Schulz, C. E.; Britt, R. D.; Power, P. P., Direct Spectroscopic Observation of Large Quenching of First-Order Orbital Angular Momentum with Bending in Monomeric, Two-Coordinate Fe(II) Primary Amido Complexes and the Profound Magnetic Effects of the Absence of Jahn− and Renner−Teller Distortions in Rigorously Linear Coordination. *J. Am. Chem. Soc*. **2009**, *131*, 12693-12702.
9. Ni, C.; Power, P. P. Insertion Reaction of a Two-Coordinate Iron Diaryl with Dioxygen and Carbon Monoxide. *Chem. Commun.* **2009**, 5543-5545.

10. Bryan, A. M.; Long, G. J.; Grandjean, F.; Power, P. P. Synthesis, Structural, Spectroscopic, and Magnetic Characterization of Two Coordinate Cobalt(II) Aryloxides with Bent or Linear Coordination. *Inorg. Chem.* **2014**, *53*, 2962-2698.
11. Ingleson, M. J.; Layfield, R. A., N-Heterocyclic carbene chemistry of iron: fundamentals and applications *Chem. Commun*. **2012**, *48*, 3579-3589.
12. Layfield, R. A.; McDouall, J. J. W.; Scheer, M.; Schwarzmaier, C.; Tuna, F., Structure and bonding in three-coordinate N-heterocyclic carbene adducts of iron(II) bis(trimethylsilyl) amide. *Chem. Commun.* **2011**, *47*, 10623-10625.
13. Neese, F.; Pantazis, D. A., What is not required to make a single molecule magnet. *Faraday Discuss.* **2011**, *148*, 229-238.
14. Sulway, S. A.; Collison, D.; McDouall, J. J. W.; Tuna, F.; Layfield, R. A., Iron(II) cage complexes of N-heterocyclic amide and bis(trimethylsilyl) amide ligands: Synthesis, structure, and magnetic properties *Inorg. Chem.* **2011**, *50*, 2521-2526.
15. Bryan, A. M.; Long, G. J.; Grandjean, F.; Power, P. P., Synthesis, spectroscopic characterization, and determination of the solution association energy of the dimer $[Co\{N(SiMe_3)_2\}_2]_2$: magnetic studies of low-coordinate Co(II) silylamides $[Co\{N(SiMe_3)_2\}_2L]$ (L = PMe_3, pyridine, and THF) and related species that reveal evidence of very large zero-field splittings. Inorg. Chem. **2013**, 52, 12152-12160.
16. Hatanaka, T.; Miyake, R.; Ishida, Y.; Kawaguchi, H., Synthesis of two-coordinate iron aryloxides and their reactions with organic azide: Intramolecular C–H bond amination. J. Organomet. Chem. **2011**, 696, 4046-4050.

17. Bartlett, R. A.; Power, P. P. Two-Coordinate, Nonlinear, Crystalline d^6 and d^7 Complexes: Syntheses and Structures of $M\{N(SiMePh_2)_2\}_2$, M = Fe or Co. *J. Am. Chem. Soc.* **1987**, *109*, 7563-7564.

18. Andersen, R. A.; Faegri, K.; Green, J. C.; Haaland, A.; Lappert, M. F.; Leung, W. P.; Rypdal, K., Synthesis of bis[bis(trimethylsilyl)amido]iron(II). Structure and bonding in $M[N(SiMe_3)_2]_2$ (M = manganese, iron, cobalt): two-coordinate transition-metal amides. *Inorg. Chem.* **1988**, *27*, 1782-1786.

19. Boynton, J. N.; Guo, J.-D.; Fettinger, J. C.; Melton, C. E.; Nagase, S.; Power, P. P., Linear and Nonlinear Two-Coordinate Vanadium Complexes: Synthesis, Characterization, and Magnetic Properties of V (II) Amides**.** *J. Am. Chem. Soc***. 2013,** *135*, 10720-10728.

20. Boynton, J. N.; Merrill, W. A.; Reiff, W. M.; Fettinger, J. C.; Power, P. P., Two-Coordinate, Quasi-Two-Coordinate, and Distorted Three Coordinate, T-Shaped Chromium (II) Amido Complexes: Unusual Effects of Coordination Geometry on the Lowering of Ground State Magnetic Moments. *Inorg. Chem*. **2012**, *51*, 3212-3219.

21. Li, J.; Song, H.; Cui, C.; Cheng, J.-P., Synthesis and characterization of linear and square-planar nickel complexes with primary amido ligands. *Inorg. Chem*. **2008**, *47*, 3468-3470.

22. Lin, C.-Y.; Guo, J.-D.; Fettinger, J. C.; Nagase, S.; Grandjean, F.; Long, G. J.; Chilton, N. F.; Power, P. P., Dispersion Force Stabilized Two-Coordinate Transition Metal–Amido Complexes of the −$N(SiMe_3)$Dipp (Dipp= C_6H_3-2, 6-Pr^i_2) Ligand: Structural, Spectroscopic, Magnetic, and Computational Studies**.** *Inorg. Chem.* **2013**, *52*, 13584-13593.

23. Ashley, A.A.: Cowley, A.R.; Green, J. C.; Johnston, D. R.; Watkin, D.J.; Kays, D.L., Characterisation of Low-Coordinate Transition Metal Complexes Stabilised by Sterically Demanding Carbazolido Ligands. Eur. J. *Inorg. Chem*, **2009**, 2574-2252.

24. Andersen, R. A.; Berg, D. J.; Fernholt, L.; Faegri, K.; Green, J. C.; Haaland, A.; Lappert, M. F.; Leung, W. P.; Rypdal, K., Monomeric, base-free Mn (II) dialkyls; synthesis, magnetic properties and molecular structure of MnR_2. *Acta Chem. Scand*. **1988**, *42*, 554-562.
25. Andersen, R. A.; Haaland, A.; Rypdal, K.; Volden, H. V., The molecular structure of monomeric base-free bis(neopentyl)manganese by gas electron diffraction. *J. Chem. Soc., Chem. Commun.* **1985**, 1807-1808.
26. Andersen, R. A.; Carmona-Guzman, E.; Gibson, J. F.; Wilkinson, G., Neopentyl, neophyl, and trimethylsilylmethyl compounds of manganese. Manganese (II) dialkyls; manganese(II) dialkyl amine adducts; tetra-alkylmanganate(II) ions and lithium salts; manganese(IV) tetra-alkyls. *J. Chem. Soc., Dalton Trans.* **1976**, 2204-2211.
27. Buttrus, N. H.; Eaborn, C.; Hitchcock, P. B.; Smith, J. D.; Sullivan, A. C., Preparation and crystal structure of a two-co-ordinate manganese compound, bis[tris(trimethyl)silylmethyl] manganese. *J. Chem. Soc., Chem. Commun*. **1985**, 1380-1381.
28. LaPointe, A. M., $Fe[C(SiMe_3)_3]_2$: synthesis and reactivity of a monomeric homoleptic iron (II) alkyl complex. *Inorg. Chim. Acta.* **2003**, *345*, 359-362.
29. Viefhaus, T.; Schwarz, W.; Hubler, K.; Locke, K.; Weidlein, J., Das unterschiedliche Reaktionsverhalten von basefreiem Tris(trimethylsilyl)methyl-Lithium gegenüber den Trihalogeniden der Erdmetalle und des Eisens *Z. Anorg. Allg. Chem*. **2001**, *627*, 715-725.
30. Kays (nee Coombs) D. L.; Cowley, A.R. Monomeric two coordinate Mn, Fe and Co(II) complexes featuring 2,6-(2,4,6-trimethylphenyl) phenyl ligands. *Chem Comm.,* **2007**, 1053 – 1055.
31. Kays D. L. The stabilization of organometallic complexes using m-terphenyl ligands. *Organometallic Chemistry,* **2010**, *36*, 56-76.

32. Wehmschulte, R.J.; Power, P.P. Synthesis and characterization of the sigma bonded quasi-linear metal (II) diaryls MMes*$_2$ (M = Mg, Mn or Fe; Mes* = C_6H_2-2,4,6-Bu$^t_3$) *Organometallics,* **1995**, *14*, 3264 - 3267.

33. Müller, H.; Seidel W.; Görls, H. Fe(2,4,6-Bu$^t_3C_6H_2)_2$ A monomeric diaryl complex with two-coordinate iron (II). *Angew. Chem. Int. Ed.,* **1995**, *36*, 325 - 327.

34. Ellison, J. J.; Ruhlandt-Senge, K.; Power, P. P. Synthesis and Characterization of Thiolato Complexes with Doubly Coordinated Iron. *Angew. Chem. Int. Ed.* **1994**, *22*, 1178-1181.

35. Nguyen, T.; Panda, A.; Olmstead, M. M.; Richards, A. F.; Stender, M.; Brynda, M.; Power, P. P., Synthesis and Characterization of Quasi-Two-Coordinate Transition Metal Dithiolates M (SAr*)$_2$ (M= Cr, Mn, Fe, Co, Ni, Zn; Ar*= C_6H_3-2, 6 (C_6H_2-2,4,6-Pr$^i_3)_2$**.** *J. Am. Chem. Soc.* **2005**, *127*, 8545-8552.

36. Laskowski, C. A.; Hillhouse, G. L., Two-coordinate d^9 complexes. synthesis and oxidation of NHC nickel (I) amides. *J. Am. Chem. Soc.* **2008**, *130*, 13846-13847.

37. Ito, M.; Matsumoto, T.; Tatsumi, K., Synthesis and Reactions of Mono-and Dinuclear Ni (I) Thiolate Complexes. *Inorg. Chem.* **2009**, *48*, 2215-2223.

38. Samuel, P. P.; Mondal, K. C.; Roesky, H. W.; Hermann, M.; Frenking, G.; Demeshko, S.; Meyer, F.; Stueckl, A. C.; Christian, J. H.; Dalal, N. S.; Ungur, L.; Chibotaru, L. F.; Proepper, K.; Meents, A.; Dittrich, B., Synthesis and Characterization of a Two-Coordinate Manganese Complex and its Reaction with Molecular Hydrogen at Room Temperature**.** *Angew. Chem. Int. Ed*. **2013**, *52*, 11817-11821.

39. Mo, Z.; Chen, D.; Leng, X.; Deng, L., Intramolecular C (sp^3)–H Bond Activation Reactions of Low-Valent Cobalt Complexes with Coordination Unsaturation. *Organometallics* **2012**, *31*, 7040-7043.

40. Arduengo, A. J.; Gamper, S. F.; Calabrese, J. C.; Davidson, F., Low-coordinate carbene complexes of nickel (0) and platinum (0). *J. Am. Chem. Soc.* **1994**, *116*, 4391-4394.

41. Caddick, S.; Cloke, F. G. N.; Hitchcock, P. B.; Lewis, A. K. D., Unusual reactivity of a nickel N-heterocyclic carbene complex: tert-butyl group cleavage and silicone grease activation. *Angew. Chem. Int. Ed.* **2004**, *43*, 5824-5827.

42. Matsubara, K.; Miyazaki, S.; Koga, Y.; Nibu, Y.; Hashimura, T.; Matsumoto, T., An Unsaturated Nickel (0) NHC Catalyst: Facile Preparation and Structure of Ni (0)$(NHC)_2$, Featuring a Reduction Process from Ni(II)(NHC)$(acac)_2$. *Organometallics* **2008**, *27*, 6020-6024.

43. Danopoulos, A. A.; Pugh, D., A method for the synthesis of nickel (0) bis (carbene) complexes. *Dalton Trans.* **2008**, 30-31.

44. (a) Radius, U.; Bickelhaupt, F. M., Coord. Chem. Rev. **2009,** *253*, 678-686. (b) Radius, U.; Bickelhaupt, F. M., *Organometallics* **2008,** *27*, 3410–3414.

45. Poulten, R. C.; Page, M. J.; Algarra, A. G.; Le Roy, J. J.; Lopez, I.; Carter, E.; Llobet, A.; Macgregor, S. A.; Mahon, M. F.; Murphy, D. M.; Murugesu, M.; Whittlesey, M. K., Synthesis, electronic structure, and magnetism of $[Ni(6\text{-}Mes)_2]^+$: A two-coordinate nickel (I) complex stabilized by bulky N-heterocyclic carbenes. *J. Am. Chem. Soc.* **2013**, *135*, 13640-13643.

46. Mondal, K. C.; Samuel, P. P.; Li, Y.; Roesky, H. W.; Roy, S.; Ackermann, L.; Sidhu, N. S.; Sheldrick, G. M.; Carl, E.; Demeshko, S.; De, S.; Parameswaran, P.; Ungur, L.; Chibotaru, L. F.; Andrada, D. M., A Catalyst with Two-Coordinate Nickel: Theoretical and Catalytic Studies *Eur. J. Inorg. Chem.* **2014**, 818-823.

47. Ohta, S.; Ohki, Y.; Ikagawa, Y.; Suizu, R.; Tatsumi, K., Synthesis and characterization of heteroleptic iron (II) thiolate complexes with weak iron– arene interactions. *J. Organomet. Chem.* **2007**, *692*, 4792-4799.

48. Pangborn, A. B.; Giardello, M. A.; Grubbs, R. H.; Rosen, R. K.; Timmers, F. J., Safe and convenient procedure for solvent purification. *Organometallics*, **1996**, *15*, 1518-1520.

49. Horvath, B.; Moseler, R.; Horvath, E. G., Manganese (II) Silylamides. *Z. Anorg. Allg. Chem*. **1979**, *450*, 165-177.

50. Sutton, A. D.; Fettinger, J. C.; Rekken, B. D.; Power, P. P., Synthesis and characterization of low valent vanadium thiolate complexes. *Polyhedron* **2008**, *27*, 2337-2340.

51. Niemeyer, M.; Power, P. P., Donor-free alkali metal thiolates: synthesis and structure of dimeric, trimeric, and tetrameric complexes with sterically encumbered terphenyl substituents. *Inorg. Chem*. **1996**, *35*, 7264-7272.

52. Betz, P.; Jolly, P. W.; Kruger, C.; Zakrzewski, U., Organochromium. π-complexes. 3. Preparation and reactions of bis (μ-3-allyl) chromium (II) complexes. *Organometallics* **1991**, *10*, 3520-3525.

53. Bürger, H.; Wannagat U., Silylamido-Derivate von Chrom, Mangan, Nickel und Kupfer. *Monatsh. Chem*. **1963,** *95*, 1099–1102.

54. Hope, H. X-Ray Crystallography: A Fast, First-Resort Analytical Tool. *Prog. Inorg. Chem*. **1995**, *41*, 1-71.

55. Sheldrick, G. M., SADABS, Siemens Area Detector Absorption Correction. In A51, Göttingen, *U., Ed. Göttingen, Germany,* **2008**; p 33.

56. Blessing, R. H., An empirical correction for absorption anisotropy. *Acta Crystallogr. Sect. A: Found. Crystallogr.* **1995**, *51*, 33-38.

57. Sheldrick, G. M., SHELXTL, Version 6.1. In Inc., B. A., Ed. Madison, WI, **2002.**

58. Dolomanov, O. V.; Bourhis, L. J.; Gildea, R. J.; Howard, J. A. K.; Puschmann, H., OLEX2: a complete structure solution, refinement and analysis program. *J. Appl. Crystallogr*. **2009**, *42*, 339-341.

59. Perdew, J. P.; Burke, K.; Ernzerhof. M. Generalized Gradient Approximation Made Simple. *Phys. Rev. Lett.* **1996**, *77*, 3865–3868.

60. Perdew, J. P.; Burke, K.; Ernzerhof. M. Erratum: Generalized Gradient Approximation Made Simple. *Phys. Rev. Lett.* **1996**, *78*, 1396–1396.

61. Ernzerhof, M.; Scuseria, G. E. Assessment of the Perdew–Burke–Ernzerhof exchange-correlation functional. *J. Chem. Phys.* **1999**, *119*, 5029–5036.

62. Adamo, C.; Barone, V. Toward reliable density functional methods without adjustable parameters: The PBE0 model. *J. Chem. Phys.* **1999**, *110*, 6158–6170.

63. Weigend, F.; Ahlrichs, R., Balanced basis sets of split valence, triple zeta valence and quadruple zeta valence quality for H to Rn: Design and assessment of accuracy. *Chem. Phys.* **2005**, *7*, 3297-3305.

64. Grimme, S.; Antony, J.; Ehrlich, S.; Krieg, H. A consistent and accurate ab initio prametrization of density functional dispersion correction (DFT-D) fort the 94 elements H–Pu. *J. Chem. Phys*. **2010**, *132*, 154104.

65. Grimme, S.; Ehrlich, S.; Goerigk, L., Effect of the damping function in dispersion corrected density functional theory. *J. Comput. Chem.* **2011**, *32*, 1456-1465.

66. TURBOMOLE V6.5 2013, a. d. o. U. o. K. a.; Forschungszentrum Karlsruhe GmbH, -.; TURBOMOLE GmbH, s. a. f.; http://www.turbomole.com.

67. Gaussian 09, Revision D.01, M. J. Frisch, G. W. Trucks, H. B. Schlegel, G. E. Scuseria, M. A. Robb, J. R. Cheeseman, G. Scalmani, V. Barone, G. A. Petersson, H. Nakatsuji, X. Li, M. Caricato, A. Marenich, J. Bloino, B. G. Janesko, R. Gomperts, B. Mennucci, H. P. Hratchian, J. V. Ortiz, A. F. Izmaylov, J. L. Sonnenberg, D. Williams-Young, F. Ding, F. Lipparini, F. Egidi, J. Goings, B. Peng, A. Petrone, T. Henderson, D. Ranasinghe, V. G. Zakrzewski, J. Gao, N. Rega, G. Zheng, W. Liang, M. Hada, M. Ehara, K. Toyota, R. Fukuda, J. Hasegawa, M. Ishida, T. Nakajima, Y. Honda, O. Kitao, H. Nakai, T. Vreven, K. Throssell, J. A. Montgomery, Jr., J. E. Peralta, F. Ogliaro, M. Bearpark, J. J. Heyd, E. Brothers, K. N. Kudin, V. N. Staroverov, T. Keith, R. Kobayashi, J. Normand, K. Raghavachari, A. Rendell, J. C. Burant, S. S. Iyengar, J. Tomasi, M. Cossi, J. M. Millam, M. Klene, C. Adamo, R. Cammi, J. W. Ochterski, R. L. Martin, K. Morokuma, O. Farkas, J. B. Foresman, and D. J. Fox, Gaussian, Inc., Wallingford CT, 2016.

68. Roos, B. O. *The Complete Active Space Self-Consistent Field Method and Its Applications in Electronic Structure Calculations in Advances in Chemical Physics: Ab Initio Methods in Quantum Chemistry II*, Vol 69. Ed. Lawley, K. P. 1987, Wiley, New York, NY, USA.

69. Roos, B. O.; Lidh, R.; Malmqvist, P. Å.; Veryazov, V.; Widmark, P.-O. *Multiconfigurational Quantum Chemistry*. 2016, Wiley, Hoboken, NJ, USA.

70. Neesem F.; Petrenko, T.; Ganyushin, D.; Olbrich, G. Advanced aspects of ab initio theoretical spectroscopy of transition metal complexes: Multiplets, spin-orbit coupling and resonance Raman intensities. *Coord. Chem. Rev.* **2007**, *251*, 288–327.

71. Angeli, C.; Cimiraglia, R.; Evangelisti, S.; Leininger, T.; Malrieu, J.-P. Introduction of *n*-electron valence states for multireference perturbation theory. *J. Chem. Phys.* **2001**, *114*, 10252–10264.

72. Angeli, C.; Cimiraglia, R.; Malrieu, J.-P. *N*-electron valence state perturbation theory: a fast implementation of the strongly contracted variant. *Chem. Phys. Lett.* **2001**, *350*, 297–305.

73. Angeli, C.; Cimiraglia, R.; Malrieu, J.-P. *n*-electron valence state perturbation theory: A spinless formulation and an efficient implementation of the strongly contracted and of the partially contracted variants. *J. Chem. Phys.* **2002**, *117*, 9138–9153.

74. Angeli, C.; Borini, S.; Cestari, M.; Cimiraglia, R. A quasidegenerate formulation of the second order n-electron valence state perturbation theory approach. *J. Chem. Phys.* **2004**, *121*, 4043–4049.

75. Douglas, M.; Kroll, N. M. Quantum electrodynamical corrections to the fine structure of helium. *Ann. Phys.* **1974**, *82*, 89–155.

76. Hess, B. A. Relativistic electronic-structure calculations employing a two-component no-pair formalism with external-field projection operators. *Phys. Rev. A.* **1986**, *33*, 3742–3748.

77. Pantazis, D. A.; Chen, X.-Y.; Landis, C. R.; Neese, F. All-Electron Scalar Relativistic Basis Sets for Third-Row Transition Metal Atoms. *J. Chem. Theory Comput.* **2008**, *4*, 908–919.

78. Neese, F. Software update: the ORCA program system, version 4.0. *WIREs Comput. Mol. Sci.* **2017**, *8*, e1327.

79. Ohta, S.; Yokozawa, S.; Ohki, Y.; Tatsumi, K., Oxido-Bridged Di-, Tri-, and Tetra-Nuclear Iron Complexes Bearing Bis (trimethylsilyl) amide and Thiolate Ligands. *Inorg. Chem.* **2012**, *51*, 2645-2651.

80. Dorfman, J. R.; Rao, C. P.; Holm, R. H. Structural Diversity of Homoleptic Ethane-1,2-Dithiolato Complexes of the First Transition Series. *Inorg. Chem.***1985**, *24*, 453-454.

81. La Macchia, G.; Gagliardi, L.; Power, P. P.; Brynda, M., Large Differences in Secondary Metal−Arene Interactions in the Transition-Metal Dimers ArMMAr (Ar= Terphenyl; M= Cr,

Fe, or Co): Implications for Cr− Cr Quintuple Bonding. *J. Am. Chem. Soc.* **2008,** *130*, 5104-5114.

82. Nguyen, T.; Merrill, W. A.; Ni, C.; Lei, H.; Fettinger, J. C.; Ellis, B. D.; Long, G. L.; Brynda, M.; Power, P. P., Synthesis and Characterization of the Metal(I) Dimers [Ar′MMAr′]: Comparisons with Quintuple-Bonded [Ar'CrCrAr']. *Angew. Chem. Int. Ed.* **2008**, *47*, 9115-9117.

83. Evans, D. F. The Determination of the Paramagnetic Susceptibility of Substances in Solution by Nuclear Magnetic Resonance. *J. Chem. Soc.* **1959**, 2003–2005.

Table of Contents Entry

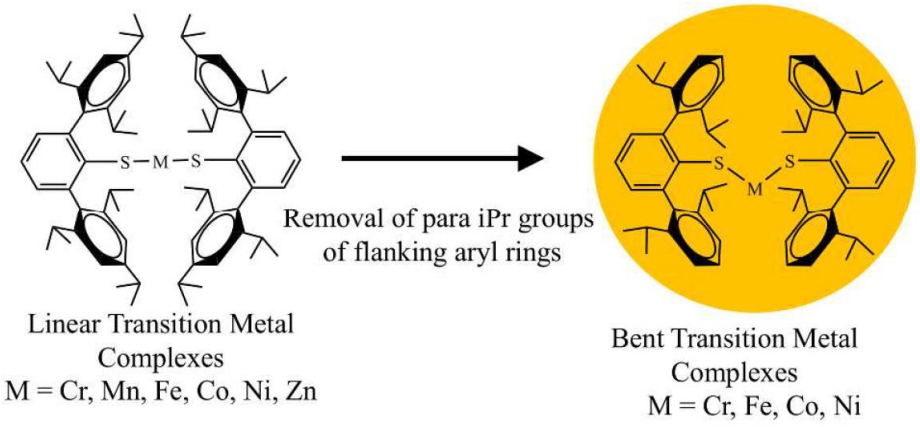

On the basis of work with earlier linear two-coordinate meal complexes of the amido (–NAr^{iPr4} and –NAr^{iPr6}; Ar^{iPr4} = C_6H_3-2,6(C_6H_3-2,6-iPr_2); Ar^{iPr6} = C_6H_3-2,6(C_6H_3-2,4,6-iPr_3) or aryloxo (–OAr^{iPr4} and –OAr^{iPr6}) ligands, it was anticipated that the thiolato ligand –SAr^{iPr4} would also induce linear or near-linear coordination, similar to that in $M(SAr^{iPr6})_2$ (M = Cr, Mn, Fe, Co, and Ni) complexes. However, it was found that the $M(SAr^{iPr4})_2$ (M = Cr, Fe, Co, and Ni) species have highly bent geometries with short metal–ligand interactions, owing to the absence of *para*-isopropyl groups on the flanking aryl rings due to the larger size of sulfur and consequent steric flexibility of the ligand.